UCLA

Title

Qualitative Analyses of Polishing and Precoating FIB Milled Crystals for MicroED

Permalink

https://escholarship.org/uc/item/5qg641kt

Journal

Structure, 27(10)

ISSN

1359-0278

Authors

Martynowycz, Michael W
Zhao, Wei
Hattne, Johan
et al.

Publication Date

2019-10-01

DOI

10.1016/j.str.2019.07.004

Peer reviewed

Qualitative Analyses of Polishing and Precoating FIB Milled Crystals for MicroED

Michael W. Martynowycz[1,2], **Wei Zhao**[3,4], **Johan Hattne**[1,2], **Grant J. Jensen**[3,4], **Tamir Gonen**[1,2,5,*]

[1]Howard Hughes Medical Institute, University of California Los Angeles, Los Angeles, CA, USA

[2]Departments of Biological Chemistry and Physiology, University of California Los Angeles, Los Angeles, CA, USA

[3]Howard Hughes Medical Institute, California Institute of Technology, Pasadena, CA, USA

[4]Department of Biology and Biological Engineering, California Institute of Technology, Pasadena, CA, USA

[5]Lead Contact

SUMMARY

Microcrystal electron diffraction (MicroED) leverages the strong interaction between matter and electrons to determine protein structures from vanishingly small crystals. This strong interaction limits the thickness of crystals that can be investigated by MicroED, mainly due to absorption. Recent studies have demonstrated that focused ion-beam (FIB) milling can thin crystals into ideal-sized lamellae; however, it is not clear how to best apply FIB milling for MicroED. Here, the effects of polishing the lamellae, whereby the last few nano-meters are milled away using a low-current gallium beam, are explored in both the platinum-precoated and uncoated samples. Our results suggest that precoating samples with a thin layer of platinum followed by polishing the crystal surfaces prior to data collection consistently led to superior results as indicated by higher signal-to-noise ratio, higher resolution, and better refinement statistics. This study lays the foundation for routine and reproducible methodology for sample preparation in MicroED.
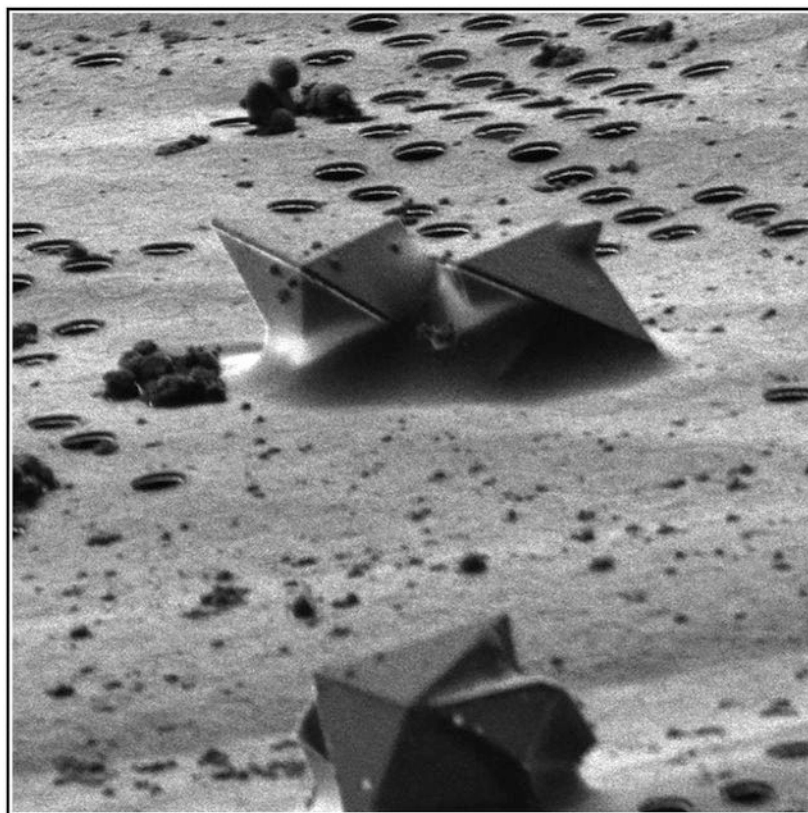
Graphical Abstract

*Correspondence: tgonen@ucla.edu.

In Brief

Low-current ion-beam polishing and precoating of crystals with a thin platinum layer are investigated and found to improve MicroED data quality. Low-dose merged structures from either coated or uncoated crystals are solved using a total exposure of only 1.5 e$^-$ Å^{-2}, and result in further improved data and structure quality.

INTRODUCTION

Focused ion beam (FIB) milling is a mature technique for shaping samples in materials science, and has recently gained popularity for preparing biological samples for investigation under a transmission electron microscope (TEM) by cryoelectron microscopy (cryo-EM) (Marko et al., 2007; Rigort et al., 2012; Wirth, 2009). Many biological samples such as cells and tissues are too thick, and would be inaccessible to investigation by a TEM without milling them down to submicron thicknesses (Marko et al., 2007). When milling, the FIB rasters back and forth across the sample to remove unwanted material. In this way, the sample and surrounding material are exposed. High-speed ions deposit some fraction of their energy into the sample due to inelastic scattering. This exposure builds up while the crystal is milled, damaging the specimen either directly from ion bombardment or through secondary effects. Furthermore, the milling process is typically conducted at grazing incidence angles of ~18°, and therefore exposes large areas of the grid around the sample to high-energy gallium ions.

To protect the sample from the ion beam, metal coating prior to FIB milling has become standard practice in FIB-scanning electron microscopy (SEM) applications. Platinum is one of the typical materials used as a coating material because of its high conductivity and contrast in electron microscopy. This additional layer protects the sample from high-energy ions during imaging with either the electron or ion beam (Rigort et al., 2012), improves contrast for biological materials, and reduces charging effects caused by the ion beams during imaging or milling (Munroe, 2009). Platinum coating may also increase the long-term stability of the grid and help preserve the specimen for future investigations.

FIB milling crystals has recently gained attention as a method for preparing samples for microcrystal electron diffraction (MicroED) experiments. MicroED is a cryo-EM technique that uses a TEM to collect electron diffraction data from nanocrystals at cryogenic temperatures (Shi et al., 2013) under continuous rotation (Nannenga et al., 2014). Electrons at commonly used accelerating voltages (80–300 kV) can only penetrate samples less than ~1 μm thickness due to the strong interaction between matter and the electron beam. Thin, uniform crystals are ideal for MicroED experiments, as this both reduces noise and eliminates the uncertainty about sample thickness (Grimm et al., 1996; Hattne et al., 2015; Martynowycz et al., 2019; Martynowycz et al., 2017). Machined crystals have been shown to retain their high-resolution information, allowing structure determination at near-atomic resolution (Duyvesteyn et al., 2018; Li et al., 2018; Martynowycz et al., 2019; Zhou et al., 2019).

The first studies on FIB milled crystals were all conducted using different experimental approaches, different samples, various detectors, and refinement software. It is, thus, unclear which approach results in the highest-quality data. For example, Duyvesteyn et al. (2018) investigated milled lysozyme crystals that had been platinum coated. Their data were collected as stills from different orientations of a single crystal, and diffraction was observed to 1.9 Å. They were able to achieve an overall completeness of 39% using a total exposure of ~25 e^- $Å^{-2}$, and used rigid body refinement to achieve reasonable structural statistics with an R_{work} and R_{free} of 29.1% and 28.3%, respectively. Li et al. (2018) also precoated their grids of lysozyme crystals with a platinum layer and similarly collected diffraction data as a sequence of still images with a total exposure of ~9 e^- $Å^{-2}$, or about 3-fold lower exposure than that of Duyvesteyn et al. (2018). Data from seven crystals were merged to solve the structure of lysozyme to 2.5 Å with an overall completeness of 94.0%. However, it appears that the model was not fully refined, and a rather high R_{free} value (~40%) was reported.

In our previous MicroED FIB milling study, we collected a continuous rotation dataset from a single proteinase K crystal to a completeness of 88% at a resolution of 2.75 Å, but the samples were not precoated with platinum (Martynowycz et al., 2019). Proteinase K was solved by molecular replacement, and refined to final R_{work} and R_{free} values of 22% and 26%, respectively, using a much lower total exposure of 4 e^- $Å^{-2}$. Later, Zhou et al. (2019) investigated lysozyme and proteinase K using an oscillation method similar to continuous rotation to solve the structures to 1.73 Å and 1.50 Å, respectively. Both of these structures were also precoated with a platinum layer, and some optimization of sample thickness was conducted. The two structures were ultimately solved using data merged using four crystals each with overall completeness of 89% (lysozyme) and 91% (proteinase), with

corresponding R_{work}/R_{free} values of 23%/25% and 19%/23%. The total exposure in this study was ~4.5 e$^-$ Å^{-2}. Importantly, these examples used different milling procedures and data-collection strategies, and it is unclear whether the resolutions and structure quality of these experiments are limited by sample, sample preparation, FIB milling protocols, radiation damage, data collection, or processing strategies.

Here we present a systematic study to evaluate the best practices for FIB milling crystals as a method for preparing samples for MicroED. Since data from each crystal were collected in the same way, we were able to perform a qualitative analysis of FIB milling procedures and evaluate how precoating grids with a thin layer of platinum and crystal polishing affect data quality.

RESULTS

Experimental Setup

Proteinase K crystals, all from the same crystallization drop, were used to create two cryo-EM grids under identical blotting and freezing conditions. One of the grids was coated with a thin layer of platinum while the other was not. These grids were then clipped and loaded on to a FIB-SEM instrument where the crystals were subsequently milled into thin ~200-nm lamellae for MicroED investigation.

Crystals were selected for milling using identical selection criteria. Namely, crystals were approximately similar in size, and were at least 20 μm away from the nearest grid bar, not within 10 μm of another crystal, and not along the milling path of another selected crystal to prevent additional exposure to the FIB. These stringent constraints reduced the number of potential crystals to ~10 crystals per grid. These crystals were milled to ~200 nm in thickness either with or without platinum coating. We ultimately collected data from eight crystal lamellae of proteinase K without platinum coating and from five lamellae with platinum coating. Grids were transferred to a TEM for MicroED data collection as previously described (Martynowycz et al., 2019). Continuous rotation data were collected from each lamella, covering a total angular range of 60° per crystal and using a total exposure of 3 e$^-$ Å^{-2}. All data were collected and processed using the same protocol, and, because the completeness from each lamella was sufficiently high, a structure could be determined from each well-diffracting lamella.

Effects of Crystal Polishing

For both the precoated and uncoated grids, we milled each crystal into a thin lamella approximately 300 nm thick. This initial milling followed our previously used protocol of slowly stepping down the beam current from >300 pA to 30 pA. For two lamellae from each grid, we continued to mill an additional ~50 nm from each side of the lamellae to reach the final thickness of 200 nm. For all of the rest of the crystals, we milled away these last 50 nm using an ultralow beam current of 10 pA to create 200-nm-thick lamellae, a process typically referred to as polishing. This current corresponds to the lowest possible setting on our FIB-SEM instrument. This step may prevent morphological pathologies in the crystals due to the

damaging nature of the high-current gallium beam, but greatly increases the amount of time it takes to reach the final lamella thickness.

Compared with polished samples, the unpolished crystals, whether coated or not, exhibit visible pathologies when imaged (Figure 1, lower left), most notably clear striations parallel to the direction of the ion beam. Crystals that were neither coated with a platinum layer nor polished resulted in either no diffraction at all or lamellae that had broken away from the grid entirely (Figure 1). For the precoated samples, some diffraction spots were observed to be split or appeared smeared, similarly to diffraction from multiple crystals. However, these reflections were ultimately integrated, with a noticeable decrease in resolution and worse merging statistics (Table 1). Internal consistency measures such as merging R factors and $CC_{1/2}$ were also worse, but that may again be a consequence of the decreased resolution.

Proteinase K Crystals Milled without Platinum Precoating

We were able to identify eight crystals that met our selection criteria from the uncoated grid. These crystals appeared to be randomly oriented upon the carbon support film. Each of these crystals was milled to a thickness of ~200 nm as detailed in STAR Methods. Of these, two were not polished and six were polished. These grids were transferred to a TEM, and continuous rotation MicroED data were collected from each crystalline lamella (Figure 1). Of these eight lamellae, four yielded clear diffraction spots, three showed no diffraction or were detached from their support, and one diffracted to ~8 Å and could not be indexed to the correct point group (Figure 1), even when enforcing the known unit cell. All four integrated datasets were sufficiently complete to allow a structure to be determined by molecular replacement using the search model PDB: 6CL7. Structures were refined in phenix.refine using electron-scattering factors, automatic solvent picking, and without any manual intervention such as modeling ions. This approach was chosen to eliminate user bias and assure proper comparisons between solved structures. A complete list of statistics is presented in Table 1. The differences in completeness for these crystals are expected, as our previous works have demonstrated that proteinase K tends to orient randomly on the grid (Hattne et al., 2016, 2018; de la Cruz et al., 2017). The average maximum resolution for these crystals was found to be 2.28 Å. The averaged, final refinements of these crystals had an R_{work} of 23.2% and an R_{free} of 28.1%, and showed no clear pathologies or issues in the densities. A typical uncoated crystal, final milled lamella, diffraction pattern, and solved structure are given in Figure 1.

Proteinase K Crystals Milled after Platinum Precoating

A second grid with crystals from the same crystallization well was prepared identically. This grid was coated in a thin layer of platinum (~50 nm) prior to being loaded into the FIB-SEM instrument. Using the same criteria as the uncoated grid, we located and milled five crystals. Three of these were polished and two unpolished, as indicated. Continuous rotation MicroED data were then collected as above. All five crystals yielded diffraction that indexed correctly. Each crystalline lamella was solved similarly to the uncoated lamellae above, and the individual statistics for these solutions are also presented in Table 1. A typical platinum-coated, polished crystal with the corresponding lamella and diffraction pattern is presented in Figure 2, alongside a typical uncoated, polished crystal. On average, these crystals

diffracted to a resolution of 1.94 Å with an R_{work} of 20.6% and an R_{free} of 24.6%. Statistics for individual platinum-coated lamellae are given in Table 1.

Dose-Fractionation Structure of Proteinase K

To compare the overall structures from both preparations with minimal TEM exposure, we merged the first half of each dataset for either the uncoated or coated lamellae that had been polished. These merged datasets were of overall high completeness and multiplicity, and were subjected to a total exposure of only 1.5 $e^- \text{ Å}^{-2}$. We refer to these as "low-dose" for the uncoated merge, and "low-dose platinum" (Table 2). The resolution for these structures was again chosen as the lowest resolution beyond which $CC_{1/2}$ was no longer significant as indicated by Student's t test at the p = 0.1 level.

It appears that precoating the samples prior to milling led to a higher-resolution structure with improved refinement statistics. We found that the low-dose uncoated dataset had a resolution of 2.16 Å with an R_{pim} of 15.3% and mean $I/\sigma I$ of 3.7, whereas the precoated dataset extended to 1.85 Å with an R_{pim} of 9.4% and mean $I/\sigma I$ of 5.4 using the same criteria. The similarities, and successful merging of these the individual crystal lamellae, indicate that there were no issues with non-isomorphism between these structures. All the relevant structural and merging statistics of this structure can be found in Table 2.

DISCUSSION

The overall statistics for each set of crystals (Figure 3 and Table 1) indicate that coating with platinum may lead to a higher success rate and result in higher-quality data. Every lamella that produced indexable diffraction in this study resulted in a high-resolution structure solution. Only half of the uncoated crystals (4/8) could be successfully processed, whereas all (5/5) of the coated crystals yielded well-refined structures (Figure 3). Two crystals from each grid were milled without a final polishing step. The coated but unpolished crystal lamellae produced diffraction that ultimately led to a structure, but these lamellae had overall poorer quality than the coated, polished lamellae (Table 1). These results are consistent with disruption of the lattice by radiation damage, resulting in diminished resolution and, thus, poorer processing statistics (Hattne et al., 2018).

Clear trends in our analysis indicate that precoating together with polishing yielded the best results. The quality metrics of success rate, maximum resolution, R_{pim}, $I/\sigma I$, number of modeled waters, and R_{free} were chosen to compare between the uncoated and precoated lamellae (Figure 3). Here, the trend is more pronounced between the different approaches. The uncoated and unpolished lamellae were completely unsuccessful and therefore omitted from the statistical results. The precoated and unpolished lamellae tended to be better than those uncoated and unpolished. The best data typically came from lamellae that were both precoated and polished (Figure 3). Although our findings demonstrate clear trends and improvements for the various FIB milling modalities, these may only apply to this specific sample, and different results may be obtained once crystal and sample variability is taken into account.

The dose-fractionated datasets created from both the uncoated and precoated, polished lamellae were of overall much higher quality than any of the individual lamellae (Table 2). Comparing individual statistics between the two merges clearly demonstrates that precoating the grids led to better-quality data. The final structure and a representative portion of the $2mF_o-dF_c$ map for the precoated, dose-fractionated proteinase K is shown in Figure 3. Continuous, unbroken density was observed for disulfide bonds, indicating that dose fractionation resulted in structures with minimal damage from exposure to the electron beam.

We chose the resolution limit of each dataset based on the significance of the $CC_{1/2}$ value (p = 0.1, Student's t test) as previously described (Evans and Murshudov, 2013; Karplus and Diederichs, 2012). Lamellae coated with platinum consistently resulted in higher resolution. Although we believe that primary gallium damage is not the culprit for the reduction of resolution, we cannot discount secondary effects that may constitute the majority of damaging events in traditional macromolecular crystallography (Garman and Weik, 2015; Hattne et al., 2018). The coating comes with the added benefits of increased contrast during the FIB-SEM stages and prevents exposure to electrons and ions during the FIB-SEM experiments. The total exposures to both sets of crystals during MicroED experiments in the TEM were identical. The stability added by the platinum layer may serve to increase the strength of the base both while it experiences a shear force from the ion beam and during the mechanical stresses of loading and unloading the sample from the FIB-SEM to the TEM. Our initial observations of lamellae breaking during the transfer process of uncoated grids would seem to support this hypothesis.

Our platinum layer (~50 nm) is significantly thinner than the carbon-rich platinum layers used in Duyvesteyn et al. (2018), Li et al. (2018), and, later, Zhou et al. (2019), where a gas-injection system was used for platinum coating. For example, the platinum thickness in Duyvesteyn et al. (2018) was estimated at 2 μm thick. A thicker platinum layer may further reduce radiation damage to the specimens from the gallium beam during the milling procedure. However, thicker layers make locating smaller crystals more difficult by washing out the fine features seen with either a thin or no platinum layer, and may even not cover the areas occluded by sharp edges as pointed out by Zhou et al. (2019). Indeed, we found that even our thin layer of platinum coating made locating crystals using FIB imaging more difficult than in the uncoated grid. We chose the thickness of our platinum layer on the basis of previous findings that suggested that these thin layers adequately protected the sample in other applications (Rigort et al., 2012). It would follow that the thicker layers would function at least as well in protecting the lamellae from similar exposures.

We did not coat our lamellae with an additional platinum layer after milling, as is common practice in preparing lamellae for imaging. This is typically done to prevent charging of the sample during imaging of the sample in the TEM (Munroe, 2009). Charging manifests as blurring of images. Diffraction is translationally invariant, and this would not benefit our lamellae. Furthermore, the resolution of our diffraction experiments is highly sensitive to sample thickness due to absorption. Any additional material added to our lamellae, particularly of a high Z material, would be detrimental to collection of MicroED data.

All the data collected in this study were of higher resolution than our previous FIB milling investigation (Martynowycz et al., 2019). In that report, the resolution was limited to ~2.7 Å using a total exposure of ~4 e$^-$ Å^{-2}. Lowering the exposure by ~1 e$^-$ A^{-2} in total could explain some of the differences, particularly at high resolution. Here, the best resolution was 1.79 Å, or about an ångström better than our previous investigation of the same sample.

We made no attempt at collecting MicroED data from crystals coated with other materials, e.g., silver, chromium, or carbon. Differences between coating material as well as material thickness may be important parameters in optimizing MicroED data quality. A thorough investigation of the effects of coating thickness and coating material are avenues for future investigations.

We investigated the effects of precoating grids with platinum and polishing milled lamellae on MicroED data quality. Our results suggest that grids precoated with a thin layer of platinum consistently improve MicroED data quality. Adding a polishing step at very low ion-beam current was necessary to observe diffraction for crystals on the uncoated grid, but did not prevent successful integration of diffraction data from precoated grids. We merged the first half of each dataset from either the coated or uncoated, polished grids to create complete dose-fractionated datasets with minimal exposure and better statistics for comparison. Even in this case, the very best uncoated crystals were of poorer overall quality than the precoated crystals. We suggest that precoating limits radiation damage to the crystals, increases the physical robustness of the preparations, and leads to improved crystallographic statistics and structure. Our results set the standard for FIB milling crystals for MicroED data collection, and should ultimately result in higher-resolution structures of better quality in future experiments utilizing FIB milling for sample preparation.

STAR★METHODS

LEAD CONTACT AND MATERIALS AVAILABILITY

Further information and requests for resources and reagents should be directed to and will be fulfilled where reasonable by the lead contact, Tamir Gonen (tgonen@ucla.edu).

METHOD DETAILS

Crystallization of Proteinase K—Proteinase K (*E. Album*) was purchased from Sigma and used without further purification. Crystals of proteinase K were grown via the sitting drop method. Proteinase K powder was dissolved in Tris-HCl 50mM pH 8.0 to a final protein concentration of 25mg mL^{-1}. Sitting drops were set in microbridges in a 24-well plate by mixing 2μL of protein solution with 2μL of 1.25M ammonium sulfate. Crystals appeared over night with high density and an average size of about 50 μm.

Sample Preparation—Protein crystals were placed on glow-discharged Quantifoil R2/2 Cu200 mesh grids by pipetting 2μL of sample directly on to the carbon side. Grids were gently blotted from the back manually for 5 seconds at 100% humidity and 4°C before plunged into liquid ethane. Vitrified grids were transferred into liquid nitrogen, and clipped prior to milling and MicroED measurements.

Ion Beam Milling of Crystalline Lamellae—All milling and coating experiments were performed using an FEI VERSA FIB-SEM instrument at liquid nitrogen temperatures. One of the grids was coated with a thin layer of platinum prior to milling and imaging using a sputter coating system built into the Quorum transfer station as previously described (Schertel et al., 2013). Thickness of the platinum layer was set to 50 nm and controlled by a calibrated sputter time for this system. This measure was verified in the FIB-SEM using the FIB images where the platinum thickness could be directly observed (Figure 2B). The average platinum thickness on the grid squares used in this study was approximately 50 nm, that agrees well with the set thickness in the sputter coater. Crystals were identified in low-magnification SEM and FIB imaging using currents of under 100pA with 100ps dwell times. Crystals were milled by rastering over the area on interest, slowly removing portions of the embedded crystals. The current was stepped down slowly from >300pA to 30pA as the thickness of the crystals decreased to ~300 nm. For unpolished lamellae, the last 50 nm on either side was removed at a beam current of 30pA to the final thickness of ~200 nm. Alternatively, to polish the lamellae, the FIB current was lowered to 10pA that was used to polish away to final 50 nm above and below the initial ~300 nm lamellae to a final thickness of ~200 nm.

Collection of MicroED Data from Milled Crystals—Grids containing milled, crystalline lamella were loaded into the FEI Talos Arctica at liquid nitrogen temperatures. MicroED data were collected as movies. The typical MicroED workflow and setup are described in detail elsewhere (Jones et al., 2018; Martynowycz and Gonen, 2018; Martynowycz et al., 2019; Shi et al., 2016). Each crystalline lamella was continuously rotated in the electron beam at a rate of $0.2° \ sec^{-1}$ for a total of 60° at an exposure of $0.01e^{-}$ $Å^{-2}s^{-1}$ for a total exposure per crystal of $3e^{-}Å^{-2}$. Frames were read out every 3 seconds using an FEI CetaD 4kx4k CMOS detector binned by 2. A select area aperture was used to reduce the contributions from the non-crystalline surroundings of the lamella.

Data Reduction and Processing—Individual diffraction frames in MRC format from the detector were converted to SMV format for processing by in-house developed software as previously described (Hattne et al., 2015). This software is freely available on our website (https://cryoem.ucla.edu/). Diffraction images were reduced, indexed, and integrated in XDS (Kabsch, 2010a), and datasets were merged and scaled in XSCALE (Kabsch, 2010b, 2010a). Structures were determined by molecular replacement in Phaser (McCoy et al., 2007) using the search model PDB: 6CL7. The R_{free} flags were copied from this model to reduce bias (Afonine et al., 2010; Hattne et al., 2018; McCoy et al., 2007). Models from molecular replacement were refined in Phenix.refine (Afonine et al., 2012) using electron scattering factors and automatic picking of solvent molecules (Afonine et al., 2012; Peng, 1998). No manual curation of the models was conducted in order to remove bias from the results.

Statistics—Number values used to calculate the statistics in Tables 1 and 2 were given by the total number of reflections and the number of unique reflections. Error bars in Figure 3A correspond to the standard error of the mean (SEM). No other statistical tests were used within the manuscript.

DATA AND CODE AVAILABILITY

The atomic coordinates have been deposited in the Protein Data Bank under ID codes 6PKJ, 6PKK, 6PKL, 6PKM, 6PKN, 6PKO, 6PKP, 6PKQ, 6PKR, 6PKS, 6PKT. Density maps have been deposited in the Electron Microscopy Data Bank under ID code EMD-20356–20366.

ACKNOWLEDGMENTS

REFERENCES

Afonine PV, Grosse-Kunstleve RW, Chen VB, Headd JJ, Moriarty NW, Richardson JS, Richardson DC, Urzhumtsev A, Zwart PH, and Adams PD (2010). phenix.model_vs_data: a high-level tool for the calculation of crystallographic model and data statistics. J. Appl. Crystallogr 43, 669–676. [PubMed: 20648263]

Afonine PV, Grosse-Kunstleve RW, Echols N, Headd JJ, Moriarty NW, Mustyakimov M, Terwilliger TC, Urzhumtsev A, Zwart PH, and Adams PD (2012). Towards automated crystallographic structure refinement with phenix.refine. Acta Crystallogr. D Biol. Crystallogr 68, 352–367. [PubMed: 22505256]

de la Cruz MJ, Hattne J, Shi D, Seidler P, Rodriguez J, Reyes FE, Sawaya MR, Cascio D, Weiss SC, Kim SK, et al. (2017). Atomic-resolution structures from fragmented protein crystals with the cryoEM method MicroED. Nat. Methods 14, 399–402. [PubMed: 28192420]

Duyvesteyn HME, Kotecha A, Ginn HM, Hecksel CW, Beale EV, de Haas F, Evans G, Zhang P, Chiu W, and Stuart DI (2018). Machining protein microcrystals for structure determination by electron diffraction. Proc. Natl. Acad. Sci. U S A 115, 201809978.

Evans PR, and Murshudov GN (2013). How good are my data and what is the resolution? Acta Crystallogr. D Biol. Crystallogr 69, 1204–1214. [PubMed: 23793146]

Garman EF, and Weik M (2015). Radiation damage to macromolecules: Kill or cure? J. Synchrotron Radiat 22, 195–200. [PubMed: 25723921]

Grimm R, Typke D, Bärmann M, and Baumeister W (1996). Determination of the inelastic mean free path in ice by examination of tilted vesicles and automated most probable loss imaging. Ultramicroscopy 63, 169–179. [PubMed: 8921626]

Hattne J, Reyes FE, Nannenga BL, Shi D, De La Cruz MJ, Leslie AGW, and Gonen T (2015). MicroED data collection and processing. Acta Crystallogr. A Found. Adv 71, 353–360. [PubMed: 26131894]

Hattne J, Shi D, De La Cruz MJ, Reyes FE, and Gonen T (2016). Modeling truncated pixel values of faint reflections in MicroED images. J. Appl. Crystallogr 49, 1029–1034. [PubMed: 27275145]

Hattne J, Shi D, Glynn C, Zee C-T, Gallagher-Jones M, Martynowycz MW, Rodriguez JA, and Gonen T (2018). Analysis of global and site-specific radiation damage in Cryo-EM. Structure 26, 759–766.e4. [PubMed: 29706530]

Jones CG, Martynowycz MW, Hattne J, Fulton TJ, Stoltz BM, Rodriguez JA, Nelson HM, and Gonen T (2018). The CryoEM method MicroED as a powerful tool for small molecule structure determination. ACS Cent. Sci 4, 1587–1592. [PubMed: 30555912]

Kabsch W (2010a). XDS. Acta Crystallogr. D Biol. Crystallogr 66, 125–132. [PubMed: 20124692]

Kabsch W (2010b). Integration, scaling, space-group assignment and post-refinement. Acta Crystallogr. D Biol. Crystallogr 66, 133–144. [PubMed: 20124693]

Karplus PA, and Diederichs K (2012). Linking crystallographic model and data quality. Science 336, 1030–1033. [PubMed: 22628654]

Li X, Zhang S, Zhang J, and Sun F (2018). In situ protein micro-crystal fabrication by cryo-FIB for electron diffraction. Biophys. Rep 4, 339–347. [PubMed: 30596142]

Marko M, Hsieh C, Schalek R, Frank J, and Mannella C (2007). Focused-ion-beam thinning of frozen-hydrated biological specimens for cryo-electron microscopy. Nat. Methods 4, 215–217. [PubMed: 17277781]

Martynowycz M, Glynn C, Miao J, de la Cruz MJ, Hattne J, Shi D, Cascio D, Rodriguez J, and Gonen T (2017). MicroED structures from micrometer thick protein crystals. BioRxiv, 152504.

Martynowycz MW, and Gonen T (2018). From electron crystallography of 2D crystals to MicroED of 3D crystals. Curr. Opin. Colloid Interface Sci 34, 9–16. [PubMed: 30166936]

Martynowycz MW, Zhao W, Hattne J, Jensen GJ, and Gonen T (2019). Collection of continuous rotation MicroED data from ion beam-milled crystals of any size. Structure 27, 545–548.e2. [PubMed: 30661853]

McCoy AJ, Grosse-Kunstleve RW, Adams PD, Winn MD, Storoni LC, and Read RJ (2007). Phaser crystallographic software. J. Appl. Crystallogr 40, 658–674. [PubMed: 19461840]

Munroe PR (2009). The application of focused ion beam microscopy in the material sciences. Mater. Charact 60, 2–13.

Nannenga BL, Shi D, Leslie AGW, and Gonen T (2014). High-resolution structure determination by continuous-rotation data collection in MicroED. Nat. Methods 11, 927–930. [PubMed: 25086503]

Peng LM (1998). Electron scattering factors of ions and their parameterization. Acta Crystallogr. A. Found. Crystallogr 54, 481–485.

Rigort A, Bauerlein FJB, Villa E, Eibauer M, Laugks T, Baumeister W, and Plitzko JM (2012). Focused ion beam micromachining of eukaryotic cells for cryoelectron tomography. Proc. Natl. Acad. Sci. U S A 109, 4449–4454. [PubMed: 22392984]

Schertel A, Snaidero N, Han H-M, Ruhwedel T, Laue M, Grabenbauer M, and Möbius W (2013). Cryo FIB-SEM: volume imaging of cellular ultra-structure in native frozen specimens. J. Struct. Biol 184, 355–360. [PubMed: 24121039]

Schrödinger LLC (2014). The PyMOL Molecular Graphics System (Schrödinger LLC).

Shi D, Nannenga BL, Iadanza MG, and Gonen T (2013). Three-dimensional electron crystallography of protein microcrystals. Elife 2013, e01345.

Shi D, Nannenga BL, de la Cruz MJ, Liu J, Sawtelle S, Calero G, Reyes FE, Hattne J, and Gonen T (2016). The collection of MicroED data for macromolecular crystallography. Nat. Protoc 11, 895–904. [PubMed: 27077331]

Wirth R (2009). Focused Ion Beam (FIB) combined with SEM and TEM: advanced analytical tools for studies of chemical composition, microstructure and crystal structure in geomaterials on a nanometre scale. Chem. Geol 261, 217–229.

Zhou H, Luo Z, and Li X (2019). Using focus ion beam to prepare crystal lamella for electron diffraction. J. Struct. Biol 205, 59–64. [PubMed: 30794865]

Highlights

- Comparison of crystal structures with or without a precoating of platinum

- Lamellae quality increased by low-current ion-beam polishing

- Low-dose merged structures with improved quality

- Ion-beam milling of macromolecular protein crystals for MicroED
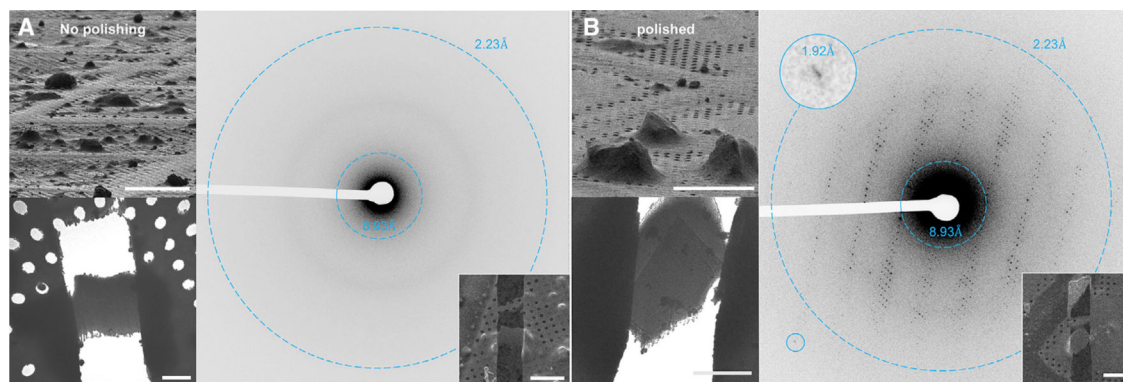
Figure 1. Uncoated Crystals with or without Polishing
The machining process of uncoated crystals without (A) and with (B) a final polishing step. Focused ion beam (FIB) images of the selected crystals before milling them down to 200-nm-thick lamellae (top left). Resulting diffraction patterns from the selected lamellae (right). Images of the final, prepared lamellae (right, inset). Clear striations and outline of the crystalline portions of these lamellae are visible in the overfocused diffraction images (bottom left). Scale bars, 50 μm (top left), 5 μm (bottom left), and 20 μm (right inset).
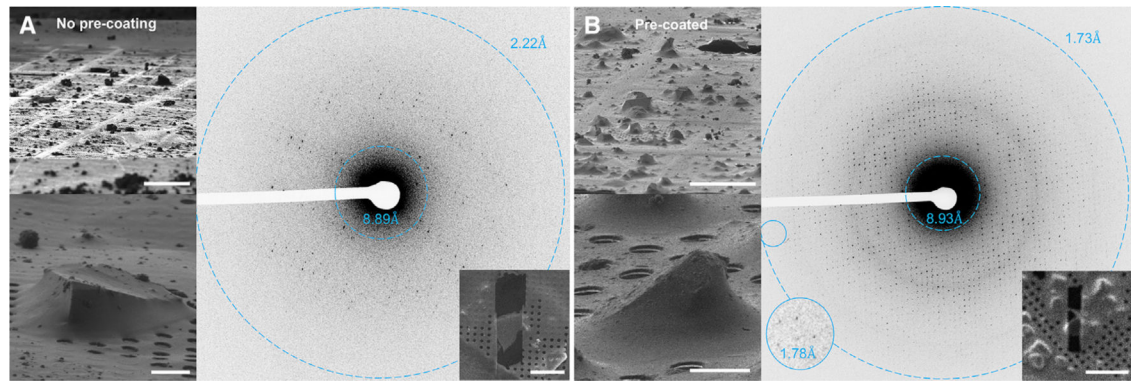
Figure 2. Platinum-Coated Crystals versus No Coating

FIB milling and MicroED data collection from grids without (A) or with (B) a thin layer of platinum precoating. Both were polished. Grid overviews (top left) show the difference in appearance in grids imaged by the FIB. Crystals prior to milling and data collection (bottom left), and the corresponding diffraction (right) from these milled lamellae (right, inset). Scale bars, 50 μm (top left), 5 μm (bottom left), and 20 μm (right inset).
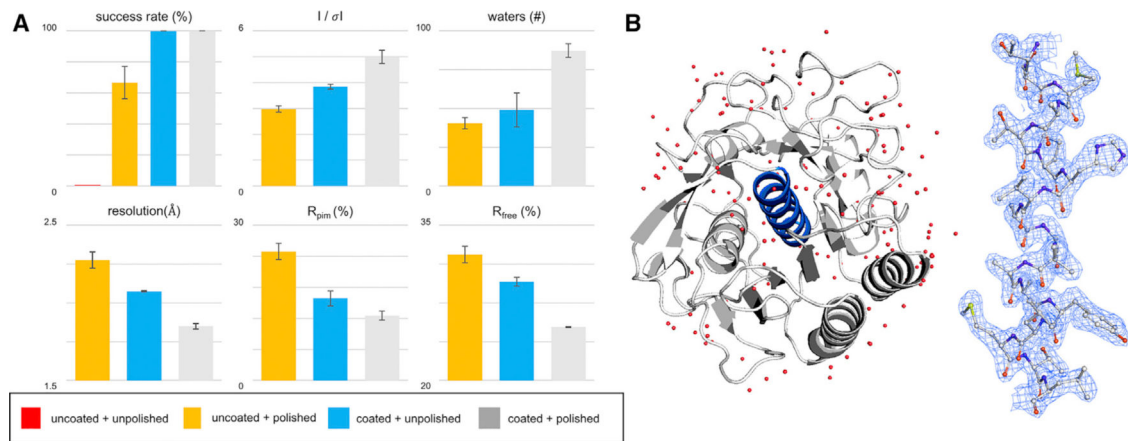
Figure 3. Comparison of Milled Lamellae

(A) Qualitative comparison of refined structure solutions from lamellae under different conditions. Coating the crystals resulted in 100% success rate. Crystals that were both platinum coated and polished consistently gave superior results with higher resolution, better signal-to-noise ratio, and better refinement statistics. Error bars correspond to the standard error of the mean.

(B) Low-dose structure of proteinase K from the platinum-coated, polished datasets. The central helix corresponding to residues 328–345 is in blue, with the corresponding $2mF_o\text{-}dF_c$ density contoured at the 1.5σ level appearing to the right of the structure.

Table 1.

Statistics and Analysis for MicroED Data Collected under Different Preparation Conditions

Parameters	Polished and Uncoated				Unpolished and Coated		Polished and Coated		
Data Collection									
Crystal #	2	5	7	8	9	12	10	11	13
Accelerating voltage (kV)	200								
Electron source	field-emission gun								
Total exposure (e⁻Å⁻²)	3								
Wavelength (Å)	0.0251								
No. of crystals	1								
Microscope	Thermo Fisher Talos Arctica								
Camera	CetaD								
Rotation rate (° s⁻¹)	0.2								
Data Analysis									
Resolution range (Å)	35.25–2.17 (2.248–2.17)	41.63–2.176 (2.254–2.18)	43.47–2.59 (2.683–2.59)	35.41–2.17 (2.248–2.17)	30.23–2.08 (2.154–2.08)	33.66–2.07 (2.144–2.07)	28.39–1.91 (1.978–1.91)	30.07–1.85 (1.916–1.85)	33.54–1.79 (1.854–1.79)
Unit cell									
$(a = b, c)$ (Å)	67.3, 104.9	67.6, 105.7	67.5, 105.2	67.5, 105.6	67.6, 104.5	67.3, 105.1	67.5, 105.9	67.2, 107.0	67.1, 107.0
$(\alpha = \beta = \gamma)$ (°)	90	90	90	90	90	90	90	90	90
Space group	$P\,4_3 2_1 2$								
Total reflections	63,495 (6,293)	63,830 (6,496)	34,844 (3,727)	61,959 (6,373)	70,454 (7,196)	60,628 (5,059)	88,818 (9,016)	99,035 (10,382)	100,799 (8,463)
Multiplicity	6.3 (6.4)	4.8 (5.0)	4.7 (5.0)	5.3 (5.6)	5.1 (5.3)	6.9 (5.9)	5.0 (5.2)	5.9 (6.3)	6.8 (5.8)
Completeness (%)	71.26	94.46	92.89	84.79	90.80	57.59	90.41	76.93	62.36
Mean $I/\sigma I$	3.38 (0.51)	2.68 (0.51)	2.49 (0.89)	3.37 (0.81)	3.65 (0.75)	4.04 (0.93)	4.16 (0.60)	4.87 (1.00)	5.95 (0.72)
Wilson B factor (Å²)	32.5	32.46	25.8	30.08	29.74	33.21	26.74	24.47	25.71
R_{pim}	0.167	0.222	0.275	0.167	0.156	0.109	0.128	0.107	0.078
$CC_{1/2}$	0.966	0.956	0.898	0.956	0.973	0.975	0.984	0.987	0.991
R_{work}	0.220	0.223	0.256	0.229	0.223	0.216	0.197	0.198	0.198
R_{free}	0.265	0.265	0.310	0.284	0.258	0.269	0.234	0.234	0.236

Table 2.

MicroED Data and Analysis from Low-Dose, Merged Crystals

Parameter	Low-Dose Uncoated	Low-Dose Precoated
Data Collection		
Accelerating voltage (kV)	200	
Electron source	field-emission gun	
Total exposure ($e^-\text{Å}^{-2}$)	1.5	
Wavelength (Å)	0.0251	
No. of crystals	4	3
Microscope	Thermo Fisher Talos Arctica	
Camera	CetaD	
Rotation rate ($^\circ$ s^{-1})	0.2	
Data Analysis		
Resolution range (Å)	41.52–2.16 (2.237–2.16)	32.08–1.85 (1.916–1.85)
Space group	P $4_3 2_1 2$	P $4_3 2_1 2$
Unit cell		
($a = b, c$) (Å)	67.5, 105.4	67.3, 106.7
($\alpha = \beta = \gamma$) ($^\circ$)	90	90
Total reflections	126,914 (12,952)	150,310 (15,323)
Multiplicity	9.4 (9.8)	7.6 (7.9)
Completeness (%)	98.87 (97.66)	90.75 (87.18)
Mean $I/\sigma I$	3.72 (0.87)	5.40 (1.14)
Wilson B factor	35.2	25.4
R_{pim}	0.153	0.094
$CC_{1/2}$	0.969	0.987
R_{work}	0.227	0.187
R_{free}	0.252	0.225

KEY RESOURCES TABLE

REAGENT or RESOURCE	SOURCE	IDENTIFIER
Chemicals, Peptides, and Recombinant Proteins		
Proteinase K	Sigma-Aldrich	Cat#P2308; CAS: 39450-01-6
Ammonium sulfate	Sigma-Aldrich	Cat#A4418; CAS: 7783-20-2
Deposited Data		
Atomic coordinates, proteinase K crystal structure used for molecular replacement	(Hattne et al., 2018)	PDB: 6CL7
Atomic coordinates and density map of proteinase K (Table 1, #2)	This paper	PDB: 6PKJ; EMDB: EMD-20356
Atomic coordinates and density map of proteinase K (Table 1, #5)	This paper	PDB: 6PKK; EMDB: EMD-20357
Atomic coordinates and density map of proteinase K (Table 1, #7)	This paper	PDB: 6PKL; EMDB: EMD-20358
Atomic coordinates and density map of proteinase K (Table 1, #8)	This paper	PDB: 6PKM; EMDB: EMD-20359
Atomic coordinates and density map of proteinase K (Table 1, #9)	This paper	PDB: 6PKN; EMDB: EMD-20360
Atomic coordinates and density map of proteinase K (Table 1, #12)	This paper	PDB: 6PKO; EMDB: EMD-20361
Atomic coordinates and density map of proteinase K (Table 1, #10)	This paper	PDB: 6PKP; EMDB: EMD-20362
Atomic coordinates and density map of proteinase K (Table 1, #11)	This paper	PDB: 6PKQ; EMDB: EMD-20363
Atomic coordinates and density map of proteinase K (Table 1, #13)	This paper	PDB: 6PKR; EMDB: EMD-20364
Atomic coordinates and density map of proteinase K (Table 2, low-dose no platinum/LD)	This paper	PDB: 6PKS; EMDB: EMD-20365
Atomic coordinates and density map of proteinase K (Table 2, low-dose with platinum/LDPT)	This paper	PDB: 6PKT; EMDB: EMD-20366
Software and Algorithms		
TVIPS tools	(Hattne et al., 2015)	N/A
XDS	(Kabsch, 2010b)	RRID:SCR_015652
XSCALE	(Kabsch, 2010a)	RRID:SCR_015652
Phaser	(McCoy et al., 2007)	RRID:SCR_014219
Phenix.refine	(Afonine et al., 2012)	RRID:SCR_014224
PyMol	(Schrodinger LLC, 2014)	RRID:SCR_000305
Other		
TEM grids	Quantifoil	N/A
easiGlow glow discharge cleaning system	PELCO	N/A
Vitrobot Mark IV plunge-freezer	Thermo Fisher	N/A
FEI Autoloader	Thermo Fischer	N/A
FEI Talos Arctica	Thermo Fischer	N/A
FEI CetaD	Thermo Fischer	N/A
FEI Versa FIB/SEM	Thermo Fischer	N/A